MAE 263F Final Report: Snake Project

Sarah Enayati and Jonathan Gray

I. INTRODUCTION

This project aims to model the undulating movements of biological snakes, enabling it to navigate and operate in challenging environments characterized by a wide range of Reynolds numbers (Re). Such environments are often inaccessible to traditional unmanned aerial vehicles (UAVs), where maneuverability and efficient movement are critical. This is especially true for microscopic motion that can be crucial for the design of drug delivery mechanisms in modern medicine. By leveraging the unique undulatory locomotion patterns of snakes, we aim to explore a design space for slender body propulsion with use of implicit time-stepping schemes and the Discrete Elastic Body (DER) method [1]. This final report details the implementation of two modeling schemes for slender body motion, Resistive Force Theory (RFT) and Slender Body Theory (SBT), compares their performance, and explores the effects of viscosity, geometric variation in the body profile, and optimal length for achieving efficient motion.

Early works by Sir Geoffrey Ingram Taylor and Professor James Gray explored ways of modeling the motion of long slender animals like snakes and worms swimming through different aqueous environments. Importantly, a clear limitation in early models was the absence of a non-empirical approach to capturing the propulsive self interaction that arises from nearby flow fields [2][3][4][5]. Such effects can be exacerbated by different characteristics of surface roughness and especially when motion occurs under low Re conditions. Since then many of research teams have built a wealth of knowledge around the more fundamental treatment of slender body motion including Gray and Hancock's development of two singular solutions to the Stokes equation [6]. From this emerged a simple algebraic model leveraging the linearity of Stokes flow for low Re applications by treating drag as anisotropic for an undulating body in a static flow field. This general treatment of motion uses so-called resistive force for net propulsion from normal components of drag which are typically treated as roughly twice the value of the tangential counterpart. Notably, the asymptotic accuracy of this approach comes from the logarithmic relationship with the body topology, namely $C_t = \frac{2\pi\mu}{ln(\frac{\lambda}{R})-0.5}$, and $C_n = \frac{4\pi\mu}{ln(\frac{\lambda}{R})+0.5}$ [7]. Long slender bodies tend toward a $\frac{C_n}{C_t}$ ratio of 2 whereas more complex bodies (where the characteristic length approaches the characteristic radius), the relative role of the tangential drag reverses and such a body can actually use aft motion to create a flow field that propels the body forward, indeed Taylor remarked on the observation of this phenomenon in nature [2]. Lighthill et al. also developed relationships for these coefficient that show some agreement with Hancock's but both implementations of resistive force theory fail when long range effects of flow field interaction combine with local effects - resistive force theory neglects long-range interactions.

Slender body theory is a more general approach to treating the drag on a body through water. Unlike RFT, SBT resolves long range hydrodynamic effects that decay with distance between any two points on the body. For generally undisturbed motion (low flexibility or high viscosity) the SBT should approach the response of RFT predictions. But when viscous contributions reduce or node-to-node proximity reduces the far-field flow interactions become more crucial. Rodenborn et al. showed how both Lighthill's and Gray and Hancock's approach to RFT fails when trying to predict the thrust and drag associated with helical flagella in fluid [8]. Such applications are relevant for microorganisms such as bacteria whose motion is governed by low Re motion and whose body has a very low characteristic aspect ratio. The long range hydrodynamics are built into SBT through the use of interaction kernels defined by some form of a Green's function summed over every interacting segment of a discretized body. The direct approach then enforces the local hydrodynamic effect from normal motion of the body onto its centerline and superposes the interaction forces along the way. Cortez et al. proposed a regularized approach to treating the interaction with the Regularized Stokeslet method, a form of SBT implementation that shows remarkable agreement with test data [9]. One key heuristic that may be problem dependent is in choosing the regularization factor - Cortez showed that typically a value of half the segment spacing works consistently for different systems, it also doubles as a physical representation of the stokeslet decaying radius [9].

In this effort, we construct an analytical framework that accurately represents snake-like undulation and the associated interactions with viscous fluids. The framework integrates both Resistive Force Theory (RFT) and Slender Body Theory (SBT) to model hydrodynamic forces, providing insights into the behavior of the robotic snake-like bodies across different fluid regimes. This dual modeling approach allows us to identify the optimal control strategies for movement, taking into account the impact of drag, bending stiffness, and fluid dynamics.

II. METHODOLOGY

The goal of this project is to simulate the locomotion of a robotic snake, using a discretized rod model to mimic the motion of a real snake. The snake's movement is modeled by applying both Resistive Force Theory (RFT) and Slender Body Theory (SBT) to understand hydrodynamic interactions in different fluid environments. We created a computational

simulation that uses both RFT and SBT to predict the movement of the snake based on various parameters, such as the length of the body, the frequency and amplitude of undulation, and the surrounding fluid's properties.

The snake is modeled as a discretized rod with multiple segments, where each segment represents a portion of the snake's body. The discretization allows the representation of the continuous body as a series of nodes, capturing the bending and undulating movements characteristic of snake locomotion. The number of segments ('nv') can be varied to control the resolution of the model, balancing accuracy and computational cost.

The head motion of the snake is applied by prescribing sinusoidal movements with defined amplitude and frequency. These parameters emulate the undulatory patterns observed in real snakes, generating traveling waves that propagate along the length of the body. The forces and resulting movements of each segment are computed based on the interaction of the snake with the fluid environment.

Two hydrodynamic models are employed to capture the interaction of the snake with the surrounding fluid. Resistive Force Theory (RFT) is used to calculate drag forces that act on each segment of the snake, assuming that each segment independently interacts with the fluid, with drag coefficients (C_t and C_n) characterizing the tangential and normal resistance, respectively. This approach provides a simplified model to approximate the local effects of drag along the body.

Slender Body Theory (SBT) is implemented to incorporate more complex hydrodynamic interactions between different segments of the snake's body. Unlike RFT, SBT accounts for the long-range influence of one segment on others by considering hydrodynamic interactions along the length of the snake. The SBT approach uses a discretized version of the Stokeslet interaction kernel to compute these forces.

The governing equations of motion for the snake are solved iteratively using a Newton-Raphson method. Forces due to bending, stretching, and hydrodynamic drag are combined to compute the net force acting on each segment. The bending and stretching energies are modeled based on the material properties of the rod, such as Young's modulus ('Y'), which controls the stiffness of the snake. The iterative solver is used to update the positions of each segment at each time step, taking into account hydrodynamic forces calculated via RFT or SBT.

We use Reynolds number to verify the validity of the SBT and RFT models in different regimes. Specifically, SBT is most accurate when the Reynolds number is low, as it assumes that inertial effects are negligible compared to viscous forces. Therefore, if the Reynolds number is found to be high and the results from SBT and RFT match closely, this suggests an inconsistency in the physical assumptions of SBT. In our project, we use the Reynolds number as a key indicator to ensure that each hydrodynamic model is used appropriately. If discrepancies arise between the predicted results from RFT and SBT at high Reynolds numbers, it indicates that the SBT model is being applied outside its valid range, and these results are examined to better understand the conditions under which each model is appropriate.

To understand the effect of various parameters on the snake's locomotion and determine optimal parameters, sensitivity analyses were performed by varying key parameters, specifically, the number of nodes and the length of the snake. These analyses help identify optimal conditions for efficient movement and quantify how different factors contribute to the dynamics of the snake. In particular, sensitivity analysis was conducted to optimize the x-velocity of the head by varying the length of the rod and the number of segments. This allowed us to determine the ideal configuration for maximizing forward propulsion, taking into account both fluid interactions and the physical properties of the snake.

A. Stability Considerations for Slender Body Theory

The SBT method is highly sensitive to both temporal and spatial discretization parameters. During our simulations, we found that achieving numerical stability with SBT required careful tuning of both the time step and the number of nodes (discretized segments of the snake's body).

Initially, we observed that SBT was prone to numerical instability, particularly for higher node counts and larger time steps. These instabilities manifested as rapidly diverging errors in the Newton solver, as well as non-physical behaviors such as unrealistic forces and velocities. To mitigate these issues, we experimented with the discretization parameters. We ultimately determined that maintaining a small time step of 0.003 and reducing the number of nodes to 3 provided a stable simulation environment for SBT.

III. Sensitivity Analysis for Parameter Determination

In our sensitivity analysis, we use the average x-direction velocity as our performance metric to evaluate the effects of different parameters (number of nodes, length of snake, and hydrodynamic influence range) on the locomotion efficiency of the robotic snake. The x-direction velocity represents the snake's forward speed, which indicates how well it can propel itself through a fluid environment using undulation.

A. Nodal Determination

We vary the number of nodes in the robotic snake to understand its effect on locomotion efficiency and average velocity and thus determine the optimal number of nodes for our snake. The number of nodes determines how well the wave propagates along the body, directly impacting the smoothness of movement and overall propulsion. As we increase the number of nodes from 5 to 25, we observe a significant improvement in average velocity [see Figure 1.] A higher number of nodes allows for smoother and more continuous undulatory movement, which generates more effective thrust. However, beyond 11 nodes, the velocity begins to plateau, with only minimal increases up to 13 nodes. This plateau suggests that additional nodes do not significantly enhance propulsion but instead add computational complexity and potentially

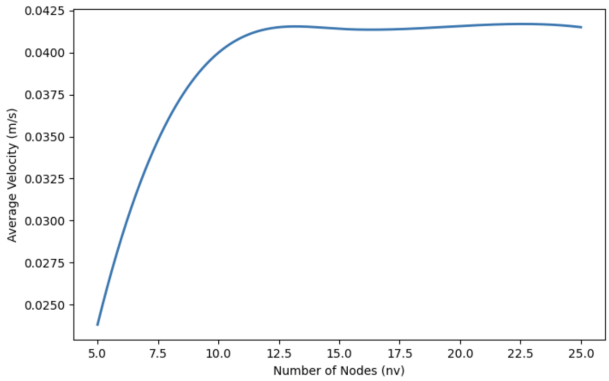

Fig. 1. Sensitivity Analysis on Number of Nodes

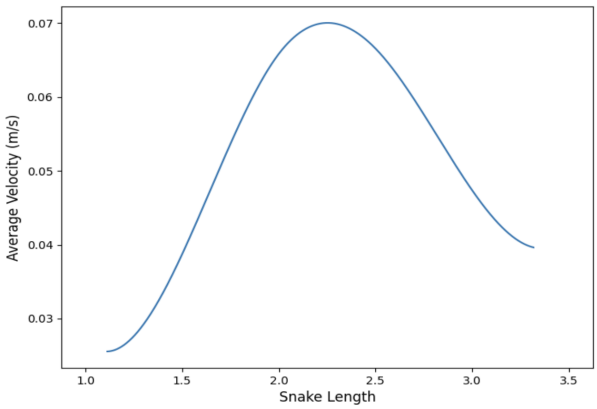

Fig. 2. Sensitivity Analysis on Snake Length

increase drag resistance. Based on these results, we choose the optimal number of nodes to be 12. This balances achieving high velocity and minimizing unnecessary computational load, and ensures efficient movement without overcomplicating the model or reducing performance due to added drag.

B. Snake Length

We also conducted sensitivity analysis on the total length of the robotic snake to understand its influence on locomotion efficiency and average velocity. The length of the snake is a critical parameter because it affects both the wave propagation dynamics and the drag experienced by the body as it moves through the fluid. A longer snake generally allows for more undulation cycles along its body, which can generate greater propulsion due to more efficient transmission of waves. However, this increased length also results in more surface area interacting with the fluid, therefore increasing drag resistance. The longer the snake, the greater the cumulative drag that each segment must overcome, which can result in decreased average velocity. On the other hand, a shorter snake experiences less overall drag, which may increase velocity, but it may also lack the sufficient wave propagation length needed to generate effective thrust. This would lead to reduced propulsion efficiency. By analyzing different snake lengths, we evaluated the

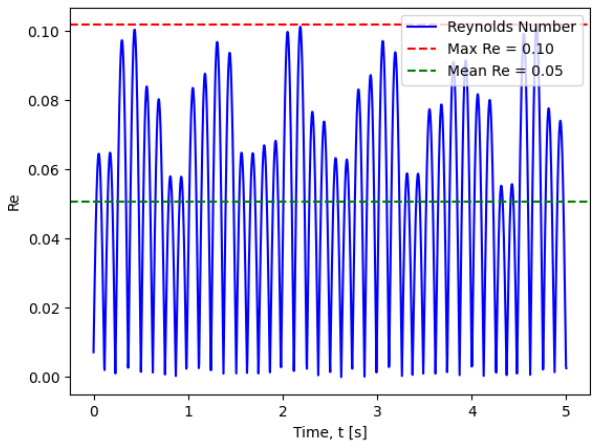

Fig. 3. Reynolds Number

trade-off between propulsion generation and fluid resistance, which allowed us to identify an optimal length that maximizes velocity while maintaining stability.

In our sensitivity analysis of the robotic snake's total length, we vary the rod length from 1.0 to 2.0 meters and observe its effect on the average velocity, as can be seen in Figure 2.

These results indicate that as the snake length increases, the average velocity initially improves, but starts declining again after reaching a peak of 2.2 meters. This is due to the increase in drag resistance as the length increases further, ultimately reaching a point where the additional surface area interacting with the fluid negates the propulsion gains. Based on these results, a snake length of 2.2 meters is optimal, as it maximizes average velocity without introducing significant drag penalties.

IV. Validation for SBT/RFT Methods

A. Reynolds Number Analysis

The code developed for this effort includes a plot output for Re as a function of time for the average body velocity. Figure 3 illustrates the mean and max Re identified during a low Re. To evaluate the behavior as Re reduces, the viscosity was increased to 1 Pa-s which is approximately the viscosity of honey. A head amplitude of 0.1 m and a frequency of 2.83 Hz was applied to the snake body simulation. The total length was set to 4 m and the radius 1 cm. The material properties used are that of Aluminum - where $\rho_{body} = 2700 kg/m^3$ and Young's Modulus is 70 GPa. At this length the natural bending frequency is between 6 and 7 Hz (approximated using $\sqrt{\frac{EI\theta}{M}}$ where $\theta = \arctan \frac{HeadAmplitude}{TotalLength}$) and therefore the applied frequency of 3 Hz is within range of flexible body dynamics. Figure 4 shows how the total displacement of the head approaches the same solution between RFT and SBT when viscosity is set to 1 Pa-s. After keeping all parameters the same and decreasing the viscosity to 0.1 Pa-s the response of the SBT simulation exhibits full damping of forward motion (-x) while the RFT simulation is still steadily moving along as

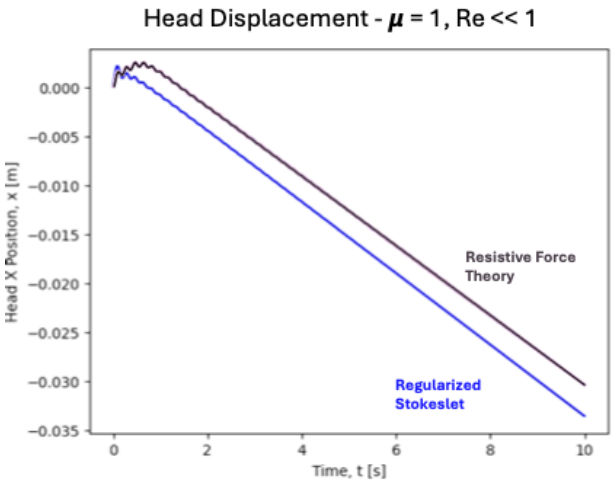

Fig. 4. X-Displacement SBT (using regularized Stokeslet) and RFT for Viscous Environment ($\mu = 1Pa - s$)

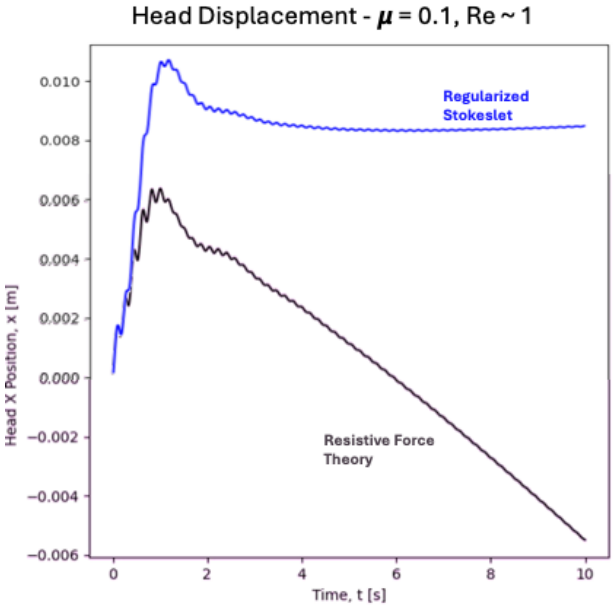

Fig. 5. X-Displacement SBT (using regularized Stokeslet) and RFT for Viscous Environment ($\mu = 0.1Pa - s$)

the head oscillates. This divergence is expected at higher Re (lower viscosity) but what was unexpected was the decrease in overall displacement for RFT. Figure 5 shows how the SBT motion comes to a halt shortly after initial excitation while the RFT motion steadily charts along -x over time at a rate of approximately 0.13 mm /s. It's not totally unexpected that the SBT motion should overall decrease with increasing Re since the flow field allows for greater local body velocity and therefore greater long range hydrodynamics, but with RFT being driven solely by local forces it was surprising to see this motion reduce. After comparing the motion of the low viscosity snake body to that of the high viscosity snake body it was apparent that a major factor in the damping of motion

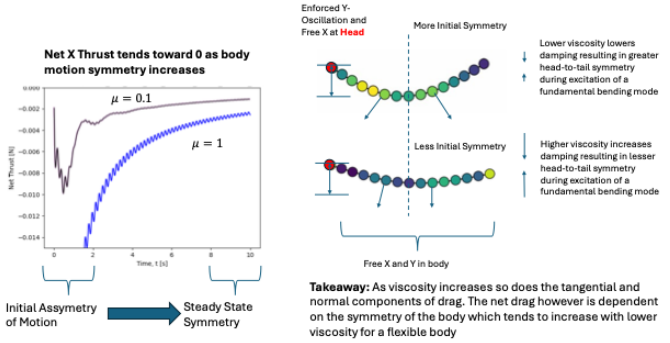

Fig. 6. Assymmetry of motion enables greater initial net thrust for the current model when viscosity is set to 1 Pa-s vs 0.1 Pa-s.

at lower viscosities was the symmetry of flexible body motion during excitation of the head node. As the y oscillation is applied, the uniform body initially exhibits asymmetry in its motion, after some time the fundamental bending mode which is near the head excitation frequency creates a standing wave which in effect zeroes out the net thrust from normal drag and the net drag from tangential drag. While this issue was discovered accidentally it does bring about some interesting conclusions about importance of asymmetry in body motion during RFT. Figure 6 shows a schematic detailing the analysis of low viscosity motion which has less damping near the tail enabling nearly perfect head-tail symmetry and high viscosity motion which has greater damping towards the tail and therefore lesser head-tail symmetry. Greater asymmetry in motion enables more efficient motion. To take this concept one step further, the code was updated to include a redistribution of mass (equal to the uniform profile model) and a gradient in radius for EA and EI variables used in elastic force extraction. In this way, there is no fundamental change or violation of the SBT theory since it is independent of geometry, however now we can explore asymmetry of the body amplitude along the length. As the profile narrows so too does the bending stiffness but at a faster rate than the discrete mass. Therefore the fundamental frequency of the system decreases as you move from a thick head to a narrow tail - this enforces body motion assymmetry with periodic head motion applied. Figure 7 shows a comparison of the performance between two equivalent models (same mass and body parameters) but with a redistribution of mass to decrease from a maximum at the head to a minimum at the tail.

Both SBT and RFT perform better when the body profile is made nonuniform but there is a clear indication of the long range hydrodynamics playing a bigger role in the body motion. The tail tends to whip around itself more with the RFT simulation of the nonuniform body while the SBT simulation reflects a noticeably more dampened y amplitude. Figure 8 shows a comparison of the greater RFT tail motion overlaid with a shadow of the equivalent SBT motion with evidence of greater long range damping.

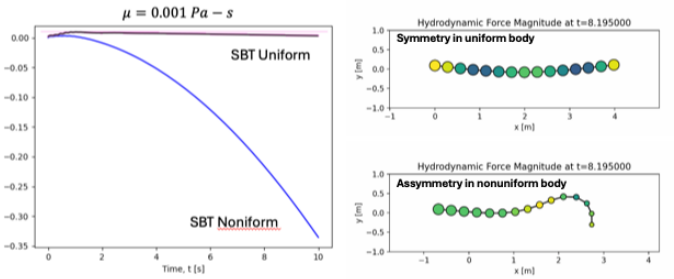

Fig. 7. Assymmetry of motion can be enforced by periodic motion at one end of an assymmetric body profile.

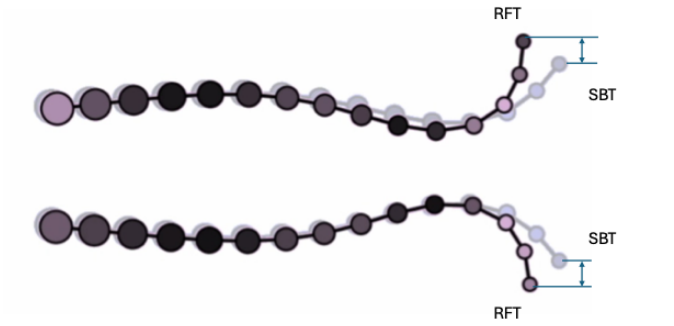

Fig. 8. Assymmetry of motion can be enforced by periodic motion at one end of an assymmetric body profile.

B. Viscosity Effects on Velocity (RFT)

We model viscosity versus velocity to validate our RFT model. The results demonstrate a clear relationship between the fluid viscosity (μ) and the average velocity of the snake's motion. Three cases were analyzed with viscosities of μ = 1.1, 1.9, and 3.0, respectively (and shown in Figures 9, 10, and 11, respectively). As viscosity increases, the absolute value of the average velocity decreases, reflecting the increased resistance of the fluid to the snake's motion. For μ = 1.1, the average velocity is -0.0513 m/s, while for μ = 1.9 and μ = 3.0, the average velocities are -0.0497 m/s and -0.0425 m/s, respectively. This aligns with theoretical expectations, as higher viscosity corresponds to greater drag forces acting on the snake.

The oscillatory behavior in the velocity profiles is also influenced by the fluid's viscosity. In lower-viscosity fluids, the velocity amplitudes are larger due to reduced resistance, allowing the snake to generate greater propulsion during its undulatory cycles. Conversely, higher viscosity dampens these oscillations, resulting in smaller amplitude variations. Despite these differences, the negative average velocity across all cases confirms consistent directional movement.

C. Net Propulsive Force Validation (RFT)

We analyze of the net propulsive forces to validate our RFT model. According to RFT, the motion of the snake generates different forces depending on the direction of movement relative to the surrounding medium. This should result in a

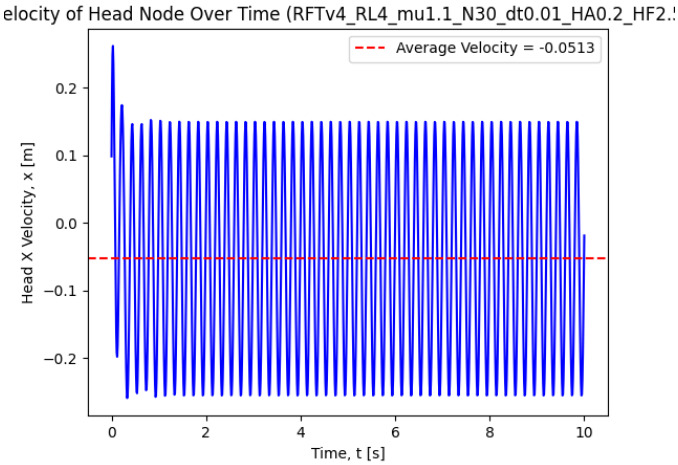

Fig. 9. Viscosity Effects on Velocity at $\mu = 1.1$

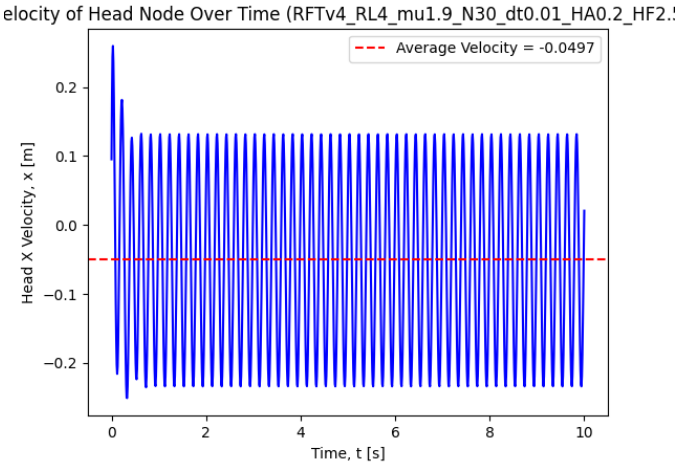

Fig. 10. Viscosity Effects on Velocity at $\mu = 1.9$

net forward force in the x-direction, while the forces in the y-direction should oscillate back and forth around zero without contributing to any net motion.

The plot of net propulsive forces matches these expectations. In the x-direction, the force oscillates over time but has a positive average, indicating that the snake is consistently moving forward. This positive average force confirms that the forward propulsion created by the snake's undulating motion is correct. In the y-direction, the forces show a clear pattern of oscillation that averages to zero, which is expected since the side-to-side motion of the snake cancels out over each full movement cycle.

The periodic nature of the forces in both directions further supports the accuracy of the model. The oscillations in the x-direction reflect the natural variation in forward thrust as the snake moves through its cycle of motion, while the y-direction oscillations capture the back-and-forth forces caused by the body's side-to-side motion. The absence of any unusual

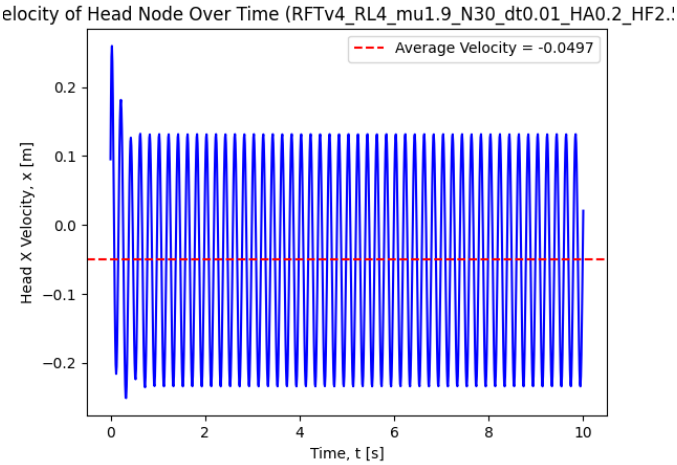

Fig. 11. Viscosity Effects on Velocity at $\mu = 3$

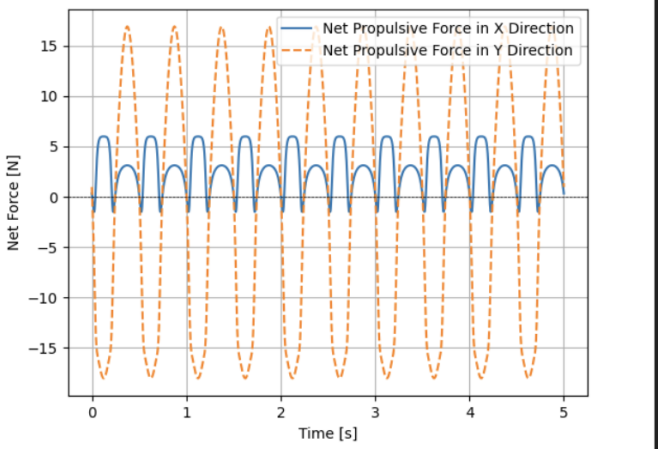

Fig. 12. Net Propulsive Forces (RFT)

trends or imbalances in the forces suggests that the model is accurately capturing the mechanics of the snake's movement.

D. Mechanical Power (RFT)

The plot of mechanical power over time serves as another important validation for the RFT model. The mechanical power reflects the work done by the snake to propel itself through its undulating motion. For the RFT model to be valid, the power should oscillate in a periodic manner, as the snake's motion involves cycles of propulsion and resistance due to the surrounding medium.

This plot exhibits the expected periodic behavior, with power oscillating between peaks and troughs. The negative values indicate that the snake is consistently expending energy to overcome drag forces, which is typical for locomotion in a resistive medium. The amplitude of the oscillations suggests that the energy expenditure varies throughout the motion cycle, with certain phases requiring more work to maintain propulsion.

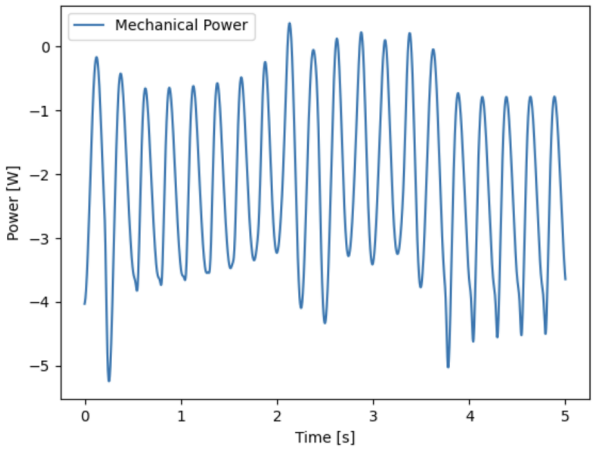

Fig. 13. Mechanical Power over Time (RFT)

The stability of the oscillations over time confirm that the model is functioning as intended. There are no irregular spikes or disruptions in the power, which would indicate numerical or modeling errors. Additionally, the gradual increase in amplitude during the initial phase of motion aligns with the expectation that the snake needs to build momentum before reaching a steady-state movement.

V. Appendix A

References

[1] Jawed, M. Khalid, Alyssa Novelia, and Oliver M. O'Reilly. \textit{A primer on the kinematics of discrete elastic rods}. Berlin/Heidelberg, Germany: Springer International Publishing, 2018.

[2] G. Taylor, "Analysis of the Swimming of Long and Narrow Animals," *Proceedings of the Royal Society of London. Series A, Mathematical and Physical Sciences*, vol. 214, no. 1117, pp. 158-183, Feb. 1952.

[3] Gray, J. 1946 J. Exp. Biol. 23, 101.

[4] Gray, J. 1939 J. Exp. Biol. 16, 9.

[5] Gray, J. Journal of Experimental Biology v. 26. 1949

[6] Gray, J., Hancock. The Propulsion of Sea Urchin Spermatozoa. 1955

[7] Coq, Naïs, et al. "Rotational dynamics of a soft filament: Wrapping transition and propulsive forces." *Physics of Fluids*20.5 (2008).

[8] Rodenborn, Bruce, et al. "Propulsion of microorganisms by a helical flagellum." Proceedings of the National Academy of Sciences 110.5 (2013): E338-E347.

[9] Cortez, Ricardo. "Regularized stokeslet segments." Journal of Computational Physics 375 (2018): 783-796.

[10] A. Yamano, K. Shimizu, M. Chiba, H. Ijima, Fluid force identification acting on snake-like robots swimming in viscous fluids, Journal of Fluids and Structures, Volume 106, 2021, 103351, ISSN 0889-9746, https://doi.org/10.1016/j.jfluidstructs.2021.103351

[11] A. Yamano, T. Kimoto, Y. Inoue, M. Chiba, Optimal swimming locomotion of snake-like robot in viscous fluids, Journal of Fluids and Structures, Volume 123, 2023, 104007, ISSN 0889-9746, https://doi.org/10.1016/j.jfluidstructs.2023.104007.

[12] Moore, B. R. (n.d.). Snake locomotion. University of Louisiana at Lafayette. Retrieved October 30, 2024, from https://userweb.ucs.louisiana.edu/brm2286/locomotn.htm

[13] Cicconofri, G., & DeSimone, A. (2015). A study of snake-like locomotion through the analysis of a flexible robot model. *Proceedings of the Royal Society A: Mathematical, Physical and Engineering Sciences, 471*(2182), 20150054. https://doi.org/10.1098/rspa.2015.0054

Algorithm 1 Get Hydrodynamic Force (getFh)

Input: $q_{new}, q_{old}, C_t, C_n, range, nv$
Output: F_{hydro}, J_{hydro}
for each node, k, in snake body: **do**
  // tangents and normals are calculated
  $\hat{t} = \frac{q_{k+1} - q_k}{|q_{k+1} - q_k|}$
  $\hat{n} = [-\hat{t}[1], \hat{t}[0]]$
  // tangential and normal velocity and forces are calculated
  $v_t = u_k \cdot \hat{t}$
  $v_n = u_k \cdot \hat{n}$
  $F_t = -C_t * v_t$
  $F_n = -C_n * v_n$
  // Hydrodynamic force is updated for all DOF
  $F_{hydro} = F_{hydro} + F_t + F_n$
  // Hydrodynamic Jacobian is updated for all DOF
  $J_t = \frac{-C_t}{dt} * \hat{t} \otimes \hat{t}$
  $J_n = \frac{-C_n}{dt} * \hat{n} \otimes \hat{n}$
  $J_{hydro}[k, k] = J_{hydro} + J_t + J_n$
  for each node, j, in range: do
    $J_{stokeslet} = \frac{(I + \hat{r} \otimes \hat{r})}{8\pi\mu|r|}$
    $F_{interaction} = J^{-1}_{stokeslet} v_{rel}$
    $F_{hydro}[k] = F_{hydro}[k] + F_{interaction}$
    $F_{hydro}[j] = F_{hydro}[j] - F_{interaction}$
    $J_{interaction} = \frac{-J_{stokeslet} \Delta L}{|r|}$
    // Update Jacobian
    $J_{hydro}[k, j] = J_{hydro}[k, j] + J_{interaction}$
    $J_{hydro}[j, k] = J_{hydro}[j, k] - J_{interaction}$
  end for
end for
$Return \quad F_{hydro}, J_{hydro}$

Algorithm 2 Snake Locomotion Simulation

Input: tol
Output: ...
$err \leftarrow \infty$
while $err > tol$ **do**
  // Stretching and bending forces calculated from predefined functions
  // Calculate viscous force and its Jacobian (using RFT)
  // Calculate hydrodynamic force and hydrodynamic interaction forces (getFh)
  $F_{hydro} = getFh(q_{new}, q_{old}, C_t, C_n, nv)$
  // Calculate Equation of Motion
  $f = M * \frac{q_{new} - q_{old}}{\Delta t^2} - M * \frac{u_{old}}{\Delta t^2} - (F_b + F_s + F_{hydro})$
end while

[14] Kimoto, T., Yamano, A., & Chiba, M. (2023). Estimation of fluid forces on a snake-like robot swimming in viscous fluids considering boundary layer thinning. In *2023 IEEE/SICE International Symposium on System Integration (SII)* (pp. 1-6). IEEE. https://doi.org/10.1109/SII55687.2023.10039336

[15] Païdoussis, Michael P., Stuart J. Price, and Emmanuel De Langre. Fluid-structure interactions: cross-flow-induced instabilities. Cambridge University Press, 2010

[16] Gray, James. "The mechanism of locomotion in snakes." Journal of experimental biology 23.2 (1946): 101-120.